Validation of the ASAR Global Monitoring Mode Soil Moisture Product Using the NAFE'05 Data Set

Iliana Mladenova, Venkat Lakshmi, *Senior Member, IEEE*, Jeffrey P. Walker, Rocco Panciera, Wolfgang Wagner, *Senior Member, IEEE*, and Marcela Doubkova

***Abstract*—The Advanced Synthetic Aperture Radar (ASAR) Global Monitoring (GM) mode offers an opportunity for global soil moisture (SM) monitoring at much finer spatial resolution than that provided by the currently operational Advanced Microwave Scanning Radiometer for the Earth Observing System and future planned missions such as Soil Moisture and Ocean Salinity and Soil Moisture Active Passive. Considering the difficulties in modeling the complex soil–vegetation scattering mechanisms and the great need of ancillary data for microwave backscatter SM inversion, algorithms based on temporal change are currently the best method to examine SM variability. This paper evaluates the spatial sensitivity of the ASAR GM surface SM product derived using the temporal change detection methodology developed by the Vienna University of Technology. This evaluation is made for an area in southeastern Australia using data from the National Airborne Field Experiment 2005. The spatial evaluation is made using three different types of SM data (station, field, and airborne) across several different scales (1–25 km). Results confirmed the expected better agreement when using point ($R_{\mathrm{station}} = 0.75$) data as compared to spatial ($R_{\mathrm{PLMR,\,1\,km}} = 0.4$) data. While the aircraft–ASAR GM correlation values at 1-km resolution were low, they significantly improved when averaged to 5 km ($R_{\mathrm{PLMR,\,5\,km}} = 0.67$) or coarser. Consequently, this assessment shows the ASAR GM potential for monitoring SM when averaged to a spatial resolution of at least 5 km.**

***Index Terms*—Advanced Synthetic Aperture Radar (ASAR) Global Monitoring (GM), National Airborne Field Experiment 2005 (NAFE'05), Polarimetric L-band Multibeam Radiometer (PLMR), soil moisture (SM), spatial variability.**

I. Introduction

THE SPATIAL and temporal resolutions at which soil moisture (SM) is observed are important preconditions when analyzing its variability. The fact that most hydrological processes are best monitored at spatial scales of 1 km or higher necessitates the need of sensors with much finer spatial resolution than the coarse resolution provided by the current and soon available passive and active microwave satellites (e.g., Advanced Microwave Scanning Radiometer for the Earth Observing System—25 km, operational since 2002; METOP Advanced Scatterometer (ASCAT)—25 km, operational since 2006; and Soil Moisture and Ocean Salinity (SMOS) and Soil Moisture Active Passive (SMAP)—40 km, scheduled for launch in 2009 and 2014, respectively). Long-term high-resolution SM monitoring by spaceborne microwave remote sensing can be achieved either by downscaling the available coarse radiometer and scatterometer estimates or by using active synthetic aperture techniques. However, there exist very few active spaceborne instruments that operate at high spatial resolution, high temporal frequency, and sensor wavelength suitable for monitoring SM.

Current operational systems are as follows: the Synthetic Aperture Radar (SAR) on RADARSAT-1/2 and ERS-1/2, the Advanced SAR (ASAR) on ENVISAT, and the Phased Array type L-band SAR (PALSAR) on ALOS; all except the last sensor operate in C-band. Operational frequency is an essential instrument characteristic since it determines the penetration depth of the microwaves in the soil profile. Currently, L-band is considered as the optimum frequency for SM monitoring due to its deeper penetration capabilities (approximately 5 cm at L-band versus 1 cm at C-band) and the reduced canopy layer attenuation. The spatial resolution of the active sensors listed earlier ranges from 10 to 1000 m. The higher spatial resolution observations that can be achieved in the finer resolution modes (SAR: fine mode—10 m; PALSAR: fine mode—7–44 m; ASAR: polarization mode—30 m) are limited in temporal repeat. Moreover, the acquisitions are irregular and often require prior request. However, frequent monitoring is essential when studying SM due to its strong temporal dynamic nature. The ASAR Global Monitoring (GM) mode offers high temporal (on average three days, including both ascending and descending orbits) and adequate spatial resolution (1 km), making it appropriate for SM studies using the temporal change detection approach.

Backscatter variability in space and the power of the returned signal are strongly influenced by the amount of vegetation on the ground, surface roughness conditions, dielectric properties of the soil, and sensor (polarization, look/incidence angle, etc.) and terrain (topography, aspect, etc.) characteristics. Moreover, the radar backscatter (σ^o) inversion for SM retrieval is generally held to be more complex than that from brightness temperature (T_B). The strong influence of the land surface on the radar measured signal and the need of ancillary data (i.e., mean square roughness height [1], surface correlation length [2], many vegetation parameters [3], etc.) make the standard retrieval algorithms applicable only to very site specific ground conditions. Consequently, there is no universal operational

Manuscript received August 22, 2008; revised February 27, 2009, July 22, 2009, and November 10, 2009.

I. Mladenova was with the Department of Earth and Ocean Sciences, University of South Carolina, Columbia, SC 29208 USA. She is now with the Hydrology and Remote Sensing Laboratory, U.S. Department of Agriculture, Beltsville, MD 20705 USA (e-mail: imladenova@geol.sc.edu).

V. Lakshmi is with the Department of Earth and Ocean Sciences, University of South Carolina, Columbia, SC 29208 USA (e-mail: vlakshmi@geol.sc.edu).

J. P. Walker and R. Panciera are with the Department of Civil and Environmental Engineering, University of Melbourne, Melbourne, Vic. 3010, Australia (e-mail: j.walker@unimelb.edu.au; rocco@civenv.unimelb.edu.au).

W. Wagner and M. Doubkova are with the Institute of Photogrammetry and Remote Sensing, Vienna University of Technology, 1040 Wien, Austria (e-mail: ww@ipf.tuwien.ac.at; mdo@ipf.tuwien.ac.at).

Digital Object Identifier 10.1109/TGRS.2010.2040746

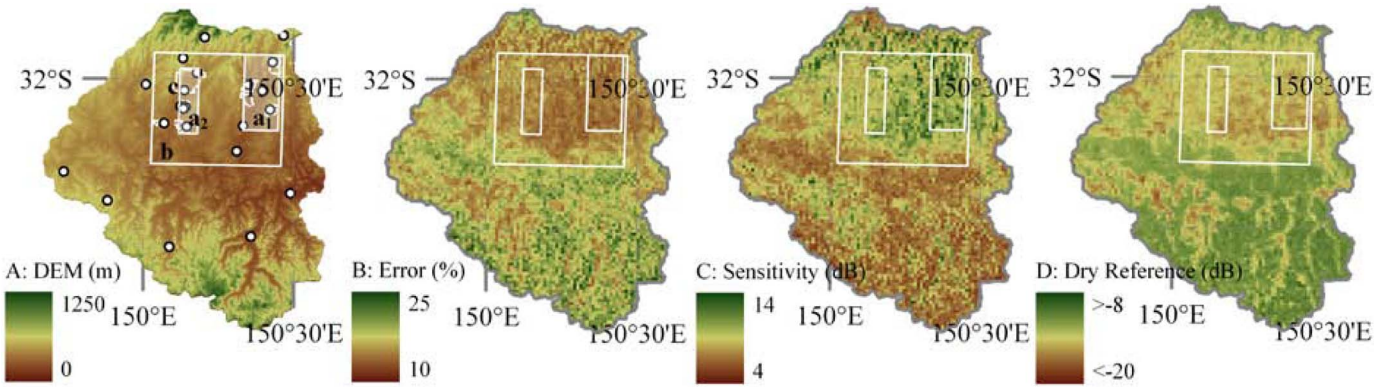

Fig. 1. Plot A shows a schematic representation of the PLMR flight within the Goulburn catchment, where a_1 and a_2 indicate the farm and **b** indicates the regional flight days. The extent of the farms sampled during the campaign is shown in the irregularly shaped polygons indicated by **c**, with the location of SM monitoring stations shown by white circles. Spatial distribution of the ASAR GM SSM model parameters is illustrated in plots B–D.

TABLE I
DAYS OF PLMR AND ASAR GM COVERAGE AND RAIN GAUGE PRECIPITATION

Date	Oct							Nov																			
	31	1	2	3	4	5	6	7	8	9	10	11	12	13	14	15	16	17	18	19	20	21	22	23	24	25
PLMR/ In situ	b	a_1	a_2	a_1	a_2			b	a_1	a_2	a_1	a_2			b	a_1	a_2	a_1	a_2			b	a_1	a_2	a_1	a_2
ASAR GM		√		√			√	√*												√*	√		√	√		
Precip (mm)	6.6	1.4	2.3	0	0	18.9	0	0	5.5	0	4.3	0	0	0	0	0.6	0	0	0	0	0	0	9.3	0.4	0	1.2

Note: b indicates 40 km x 40 km PLMR regional flight coverage, a_1 and a_2 show fine-scale sampling days (see figure 1, plot A) and √ indicates days with ASAR availability. Not all ASAR GM scenes for the NAFE'05 duration had full coverage (* - partial coverage); please note that partial coverage was determined based on comparison to the PLMR regional flight box coverage and not to the farm-scale flight boxes. However, due to the limited number of days with coincident ASAR – PLMR observations, two additional ASAR – *in situ* or PLMR pairs were used in the analysis, being November 18th-19th and 20th-21st.

algorithm for retrieval of absolute SM from the radar systems listed previously [4].

A relative surface SM (SSM) product has been developed by the microwave remote sensing group (http://www.ipf.tuwien.ac.at/radar) in the Institute of Photogrammetry and Remote Sensing, Vienna University of Technology (TU Wien). The 1-km product is derived using the ENVISAT/ASAR GM mode and represents the degree of saturation of the top surface layer [5] computed by relating the actual observed backscatter value for a particular pixel to reference backscatter values for dry and wet surface conditions. This methodology has been successfully applied for SM retrieval at 25-km resolution using scatterometer observations from ERS-1/2 and ASCAT [5]–[9]. However, at 1-km scale, the methodology has been validated only using point data, and the ASAR GM SSM 1-km product, which is used in this paper, is a new development. If proven accurate and sensitive to SM variations, the ASAR GM SSM product would be beneficial in terms of the following: 1) direct SM monitoring at a resolution suitable for local and watershed applications; 2) potential use in combined passive–active disaggregation methods [10]; and 3) improved spatial hydrologic modeling via data assimilation, rather than the commonly used approach of assimilating station-observed SM or low-resolution satellite estimates [11]–[16].

The objective of this paper is therefore to evaluate the TU Wien ASAR GM SSM product (ASAR GM SSM) using the National Airborne Field Experiment 2005 (NAFE'05) data set. The ASAR GM spatial sensitivity to SSM is assessed using the following: 1) *in situ* data from permanent SM stations; 2) extensive ground-measured SM collected during the NAFE'05 field experiment; and 3) airborne SM derived from the Polarimetric L-band Multibeam Radiometer (PLMR) at 1-km resolution. This allows the spatial sensitivity of the ASAR GM product to be analyzed over several different spatial scales and addresses an important question: Are point measurements of SM adequate to achieve accurate validation of a satellite-derived product?

II. SM DATA SETS

The NAFE'05 experiment was conducted in the Goulburn catchment (Fig. 1) during the month of November 2005 [17], [18]. The area is historically characterized by temperate climate with maximum average temperatures and major precipitation events occurring typically during the southern hemisphere summer (November to February). The field campaign sampling was undertaken over a 40 km × 40 km experimental area located in the upper half of the catchment, herein referred to as the PLMR regional flight box (Fig. 1, plot A, polygon b). The area is predominantly grasslands and croplands on undulating to flat terrain with fertile basaltic soils. Forests and sandstone-derived soil cover the southern portion of the domain. Extensive SM mapping through microwave techniques and *in situ* ground monitoring were undertaken simultaneously at several different scales (Table I and Fig. 1, plot A). Additional SM information

was available from 18 permanent stations that were present in the regional box.

The following section describes the three SM data sets (*in situ* (field and station), PLMR, and ASAR GM) used in this paper and provides an overview of the methodologies utilized in the aircraft (PLMR) and satellite (ASAR GM) retrievals.

A. In Situ SM Data Sets

The Goulburn catchment has an extensive SM and meteorological network offering near-real-time *in situ* observations since September 2002 [19]. There are 26 SM monitoring stations throughout the Goulburn catchment (white circles in Fig. 1, plot A), with 18 of them falling within the PLMR regional flight box and considered in this paper. Apart from the seven stations concentrated over an intensively monitored 150-ha area (Fig. 1, plot A, PLMR subarea a_1, middle dashed outlined polygon), the rest are evenly distributed throughout the sampling domain. Soil wetness information is recorded every 20 min at several different depths using Stevens Hydraprobes (0–5 cm) and Campbell Scientific CS616 reflectometers (0–30, 30–60, and 60–90 cm). Temperature probes, necessary for correction and calibration of the SM readings, were installed at various depths along with the SM sensors and record soil temperature data at the same time interval as the SM sensors. Considering the shallow penetration capabilities of microwave measurements, only calibrated near-SSM information from the shallowest available depth (0–5 cm) is used here. Two automated weather stations provide additional meteorological parameters (including air temperature, relative humidity, wind speed and direction, solar radiation, and barometric pressure) measured every 1-min and averaged over 20-min intervals [19].

The ground component of the NAFE'05 field campaign included 20 days of *in situ* SM sampling carried out over a 26-day period between October 31 and November 25, 2005 at two different scales—regional- and fine-scale farm samplings. The regional ground sampling was performed once a week over a 40 km $\times$ 40 km area (Fig. 1, plot A, polygon b) at approximately 1-km spacing between the sampling points. The locations of the sampling points were selected on the basis of being representative and spatially comprehensive. Farm-scale SM sampling, done twice a week, was conducted over two subareas (10 km $\times$ 30 km and 15 km $\times$ 30 km shown in Fig. 1, plot A, polygons a_1 and a_2, respectively) covering a total of eight focus farms (Fig. 1, plot A, polygon c). The fine-scale sampling scheme involved SM monitoring at several different resolutions ranging between 6.25 m in the inner most sections and 500 m in the outer most sections of the high-resolution areas (see Table I for the total number of days sampled in each land unit). The sampling distance over these areas was determined based on the local variability in terms of vegetation cover, soil type, and microtopography. The SM estimates of the top 5 cm of the soil profile were measured using Stevens Hydraprobes[1] which was done over a 6–8-h time window ($\sim$6 A.M. to $\sim$2 P.M.). Schematic representations of the *in situ* regional and farm sampling strategies are given in [18, Figs. 1 and 2].

Additional data acquired during NAFE'05 include the following [17]: gravimetric samples, collected together with the SM sampling, for calibration of the Hydraprobe readings and soil texture analyses; canopy characteristics (i.e., type and height) and vegetation samples done once a week; and surface roughness measurements, approximate percent rock cover estimates, and canopy descriptors (i.e., leaf area index) acquired once for the duration of the experiment. The vegetation data were used to monitor the spatial variability and temporal changes in vegetation water content and biomass across the domain for the duration of the campaign, as well as to provide the required vegetation parameters necessary for the retrieval procedure.

B. PLMR-Derived SM

The PLMR instrument flown on a small aircraft operates at 1.413 GHz (L-band), with both H- and V-polarizations at incidence angles of $\pm 7^\circ$, $\pm 21.5^\circ$, and $\pm 38.5^\circ$. A total of 4 regional- and 16 farm-scale (8 at each focus farm) PLMR scenes at 1-km spatial resolution were acquired coincident with the ground sampling over the three domains discussed earlier and shown in Fig. 1. Brightness temperature data were collected at 62.5-m and 1-km spatial resolutions over 4–5-h time period starting at approximately 0600 A.M.. Considering the fact that SM changes on a diurnal basis, it is important to note that the SM variability during the ground sampling time frame was estimated to be less than 0.011 $\mathrm{m}^3/\mathrm{m}^3$. Since the aircraft time period was generally shorter, that change would be even smaller for the PLMR mapping interval [18]. Along with the in-flight calibration checks, PLMR was calibrated on a daily basis both before and after the flights against cold and warm surfaces. The T_B accuracy over the 150–300 K range (T_B range measured during the campaign) was estimated to be better than 0.7 and 2 K for the H- and V-polarizations, respectively. The T_B patterns at 1-km spatial resolution over the study domain indicated good PLMR sensitivity to ground variability in terms of vegetation, SM, and topography [18], [21].

The PLMR SM product was derived using the L-band Microwave Emission of the Biosphere (L-MEB) model [22] where the land surface emission was simulated using the radiative transfer equation with vegetation assumed to be homogenous within the satellite footprint [18]. The soil–vegetation effects on the microwave signal are described using the "$\tau-\omega$ model" [23] where the T_B for certain observation angle and polarization is modeled as a function of the effective temperatures of soil and vegetation, the single scattering albedo (ω), the transmissivity of the canopy layer, and the soil reflectivity. The effective soil temperature in the model is estimated using physical temperature observations measured at the soil surface and a deep soil layer [18]. L-MEB employs two dielectric-mixing models for relating the smooth soil reflectivity to SM: Dobson [24] and Mätzler [25]; the latter is utilized for very dry soils with a sand fraction greater than 90%.

Initial retrieval was carried out using the "default" set of SMOS parameters for ω, H_r (surface roughness), and

[1]The University of Melbourne, Melbourne, Australia, has developed a technique that integrates the Stevens Hydraprobe and a Global Positioning System in a Geographical Information System framework, known as the *Hydraprobe Data Acquisition System*. It allows SM, soil temperature, auxiliary information, and exact geographic coordinates of the sampling point to be automatically recorded [20].

b (vegetation parameter) [18], [22] and utilizing 62.5-m H-polarized T_B data. Since the retrieval error was estimated to be better than the SMOS-aimed accuracy of 0.04 m^3/m^3 only for areas covered by grasslands ($RMSE_{\text{grassland\_no\_litter}} = 0.016$ m^3/m^3 and average $RMSE_{\text{grassland\_with\_litter}} = 0.041$ m^3/m^3 versus $RMSE$ over agricultural fields ranging between 0.099 and 0.325 m^3/m^3, where $RMSE$ is the root mean square error), a site-specific calibration of b and H_r was performed using field-collected vegetation and surface roughness data. The optimization was carried out through the so-called interactive least square minimization of the cost function procedure. First, b and H_r were calibrated simultaneously. Second, H_r was calibrated alone assuming that the SMOS vegetation values were correct. Third, H_r calibration as a function of SM was performed. $RMSE$ significantly improved after applying the third optimization scenario (~ 0.04 m^3/m^3 over both grass and croplands at 62.5-m resolution). The third calibrated model was subsequently applied to the 1-km PLMR retrieval. The 1-km estimates showed similar accuracy to the 62.5-km retrievals (average $RMSE_{\text{PLMR, 1 km}}$ of 0.038 m^3/m^3 and R^2 of 0.88, R. Panciera personal communication) when compared with the available ground measurements. Detailed discussion of retrieval methodology, including "default" and postcalibration parameter values and spatial accuracy of PLMR-retrieved maps over the NAFE'05 domain, is offered in [18].

C. ASAR GM SSM Product

ENVISAT is in a sun-synchronous orbit with a repeat cycle of 35 days. It crosses the equatorial plane at 10 A.M./P.M. and provides 14 orbits per day. ASAR operates at C-band with five polarization modes (VV, HH, VV/HH, HV/HH, or VH/VV) and different spatial resolutions, ranging from a couple of meters in the image mode to 1 km in the GM mode. Incidence angle ranges between 20° and 40°. Temporal resolution of the ASAR GM mode depends strongly on the geolocation of the imaging area. Typically, acquisitions are more frequent over the high-latitude areas (see Fig. 1[26]). Full description of all ENVISAT/ASAR operational products can be found at http://envisat.esa.int/instruments/asar/. Although ENVISAT has acquired data since March 2002, the GM mode data are available only from December 2004.

The product used in this paper is a relative measure of SM in the top few centimeters of the soil layer [5], [6]. The retrieval algorithm is based on temporal change detection. ASAR GM HH-polarization backscatter data are initially normalized to a medium incidence angle of 30°, where the reference angle is determined such as to minimize the extrapolation errors. It is known that backscatter is highly sensitive to water present in both the canopy and the top few centimeters of the soil layer where the SM signal has been demonstrated to dominate at lower incidence angle and observational frequency, and horizontal polarization. In change detection approaches at constant incidence angle and polarization, any change in the observed backscatter is expected to be due to changes in vegetation and/or SM. Canopy changes over longer time scales (excluding rapid events such as clearings, harvesting, etc.), as compared to the SM, and can be ignored if the change detection approach is based on relatively short time steps [10]. In the case of long-term time-series-based approaches, as in the TU Wien algorithm, the seasonal vegetation variability needs to be accounted for. However, Pathe *et al.* [26] concluded that, over the ASAR GM incidence angle range, the backscatter variability is primarily dominated by the SM signal, which supports the earlier conclusion in [8] that, at C-band, the seasonal vegetation effect is small. Thus, in a first approximation, it was neglected in the ASAR GM retrieval. The error resulting due to this simplification will be discussed in Section III-A.

The SSM (m_s) is computed by comparing the normalized backscatter value for a particular pixel to the driest and wettest measured values [see (1)], where the highest and lowest values were determined using time series analyses on a per-pixel basis. Consequently, the m_s value, which ranges between 0 (dry) and 1 (fully saturated soil), is computed by

$$m_s(t) = \frac{\left[\sigma^o(30,t) - \sigma^o_{\text{dry}}(30)\right]}{\left[\sigma^o_{\text{wet}}(30) - \sigma^o_{\text{dry}}(30)\right]} \tag{1}$$

where m_s is relative SSM content at certain time (t) and σ^o_{wet} and σ^o_{dry} are minima and maxima backscattering values at a local incidence angle of 30°. To determine the σ^o_{wet} and σ^o_{dry} values, it is assumed that the expected number of observations acquired under dry/wet SM conditions is known. Historical ERS data and thresholds of 5% and 95% SM for the dry and wet references, respectively, are used to approximate the probable number of observations. The σ^o_{dry} value, for example, is then computed by dividing the average lowest measured ASAR GM σ^o (30) by the number of estimated dry observations. Considering that atmospheric and hydrological processes are the controlling factors that affect the spatio-temporal distribution of the SM [27], the spatial resolution difference between ASAR GM and ERS is not believed to be an issue in the calibration scheme. More problematic are the limited number of ASAR observations, their irregular temporal sampling, and their high noise level [26]. These effects may lead to inaccuracies in σ^o_{wet} and σ^o_{dry} and hence to bias the retrieved SM data. The difference between the wet and dry reference values [denominator in (1)] is referred to as backscatter sensitivity (S) to SM. The σ^o_{dry} and S dependence on surface roughness and vegetation characterizes with strong spatial variability, which was discussed in details in [26].

The algorithm performance is evaluated using [26]

$$\Delta m_{s,\max} \approx \sqrt{\left(\frac{1.2}{S}\right)^2 + \left(\frac{\beta}{S}\right)^2 + 0.01} \tag{2}$$

where $\Delta m_{s,\max}$ is the maximum error, 1.2 is the sensor noise given in decibels, S is the sensitivity, and β is the slope of the σ^o-incidence curve measured in decibels per degree. This error estimate assumes maximum contribution error of the model parameters, including sensor noise, and accounts for the neglection of the seasonal vegetation effect, and inaccuracies in the dry and wet references.

The TU Wien retrieval methodology has been successfully applied to ERS and, recently, to MetOp-A ASCAT [9], [28] scatterometer data on a 25-km spatial grid and validated over the Canadian prairies [6], Iberian Peninsular [6], Ukraine [8],

and Western Africa [5]. The authors reported adequate changes in SM with change in precipitation conditions over the areas with accuracy of ∼0.048–0.063 m^3/m^3 depending on rainfall, vegetation cover, local microrelief, and soil layer depth of ground observations. Pathe *et al.* [26] present validation results over the Oklahoma MESONET, using ASAR GM, ERS, and *in situ* SM products. Taking into account the significant pixel resolution differences among all three data sources (1 km, 50 km, and point observation, respectively), the correlation coefficients obtained were interpreted as promising. However, to date, ASAR GM validation has been mostly undertaken using station data. The PLMR-retrieved SM over the NAFE'05 domain at the same resolution as ASAR GM provides a unique opportunity to address spatial validation of the ASAR GM SSM on a pixel-by-pixel basis, allowing the ASAR GM SSM spatial patterns to be studied over an area of ~ 1600 km^2 without introducing any bias that might exist from point-based monitoring due to ground heterogeneities.

The m_s value estimated by the ASAR-GM-observed backscatter using (1) is a relative measure of the moisture content in the top few centimeters of the soil layer. To perform comparison analyses with ground-measured or PLMR-retrieved SM, the m_s values were first converted into absolute SM. The conversion was done by using the van Genuchten formula [29], which relates the degree of saturation to the actual SM content. The saturated moisture content was assumed to be equal to the porosity value, which was derived in terms of soil bulk density and density of the soil particles [30]. Finally, m_s was transformed into SM by rearranging the aforementioned relationships [29], [30] to yield

$$SM = m_s \left[\left(1 - \frac{\rho_b}{\rho_s} \right) - \Theta_r \right] + \Theta_r \tag{3}$$

where m_s is the level of saturation estimated from the ASAR GM measurements, Θ_r is the residual SM, and ρ_b and ρ_s are the soil bulk density and density of soil particles (later assumed to be equal to 2.65 g/cm^3), respectively. Here, Θ_r was determined as an average of the minimum observed SM from all permanent SM stations within the 40 km × 40 km PLMR flight box ($\Theta_r = 0.04$ m^3/m^3). The average bulk density was calculated from *in situ* measurements made during the field campaign ($\rho_b = 1.08$ kg/m^3).

III. Discussion

Accuracy of the ASAR-GM-derived SM was validated at several scales: point using *in situ* observations and 1–25 km using airborne-derived SM from the PLMR L-band radiometer. The results from these validations are presented and discussed separately in Sections III-B and C. However, in order to adequately interpret the evaluation result, it is important that we first briefly describe the model parameters utilized in the ASAR GM SSM retrieval and possible error sources.

A. ASAR GM SSM—Model Parameters

The main sources of retrieval error in the ASAR GM product were the limited number of observations used in the time series, uncertainties in the statistical methods used to derive the model parameters, and the measurement noise of the ASAR system [26]. The spatial distribution of the model parameters (S and dry reference) and the maximum retrieval error over the Goulburn catchment are shown in Fig. 1 (plots B–D). Comparison of the three images revealed close spatial resemblance, which, in turn, strongly mimicked the vegetation conditions encountered in the domain. A high σ^o sensitivity range is a necessary precondition for a good algorithm performance. The spatial correlation between S and σ^o_{dry} was high ($R_{\mathrm{PLMR}} = 0.76$ and $R_{\mathrm{Goulb.Catch.}} = 0.74$) with comparable magnitude to the value reported by Pathe *et al.* [26]. The similarity of the correlation values computed over the PLMR flight box and the Goulburn catchment indicated that the PLMR extent adequately captured the spatial heterogeneity in terms of vegetation diversity and topographic variability present in the catchment. Approximately 47.5% change in SM generates 8–9-dB increase in backscatter [31]. Comparison with the sensitivity range ($S_{\mathrm{avr}} = 9.4$ dB and ∼40% SM change) over the NAFE domain revealed excellent ASAR GM sensitivity and high accuracy of the TU Wien S model parameter. Considering the three vegetation classes (forest, crops, and pasture) used in the PLMR SM retrieval (see [18, Fig. 1]), an average maximum retrieval error of 0.17 m^3/m^3 was achieved over areas covered by forests (sensitivity range of 7.7 dB), as compared to 14% and 15% for areas occupied by croplands and pastures, respectively (sensitivity range of 9.8 dB for both classes). Larger than 20% maximum error was observed over the more densely vegetated southern portion of the catchment, which agreed with the results presented in [26]. Analysis of the error budget reveals that the retrieval error is dominated by the noise of the backscatter measurements [first term in (2)], while potential errors due to seasonal vegetation cover effects are about one order of magnitude smaller.

B. ASAR GM SSM—Station/In Situ SM Comparisons

During the NAFE'05 campaign, the regional-scale *in situ* data collection was undertaken in an irregular pattern with ground spacing between the sampling points ranging between 1 and 2 km, depending on accessibility throughout the study area. The overall Pearson correlation coefficient (R) for the PLMR regional flight box is shown in Fig. 2 (plot 1a) ($R = 0.61$ and $RMSE = 0.14$ m^3/m^3). This R value was calculated using all matching dates of observations between ASAR and *in situ* data (Table I). One additional pair was included: Since the ASAR data on November 20th were acquired at ∼2300 P.M. local time, the November 21st sampled SM was paired with the November 20th ASAR GM SSM as no rainfall occurred between the time of sampling/PLMR flight and ASAR overpass.

As explained, the sampling resolution at regional and farm scales was different. The finer sampling scheme adopted on the farm-scale days meant more sampling locations, and therefore, more measurements were averaged to create the 1 km × 1 km grid across the focus farms; one may therefore assume a more accurate SM estimation on the farm- than on regional-sampling days. However, the R-values (Fig. 2, plots 1b and 1c) for the two scales ($R_{\mathrm{regional}} = 0.64$ and $R_{\mathrm{farm}} = 0.55$) were not very different compared to the overall R value for the whole domain.

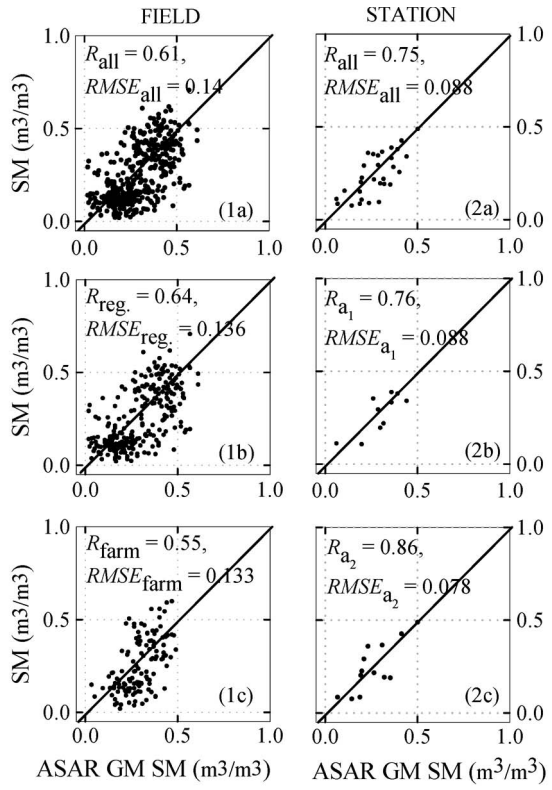

Note: $n_{(1a)}$ =411, $n_{(1b)}$ = 263, $n_{(1c)}$ = 125, $n_{(2a)}$ = 29, $n_{(2b)}$ = 11, and $n_{(2c)}$ = 13, where n is number of observations. All correlation values are significant at p = 0.01.

Fig. 2. *In situ* versus ASAR GM SSM. Columns 1 and 2 show *in situ* SM measurements averaged from field measurements gridded to 1 km and point station data, respectively. Row a is ASAR data from all flight days during the campaign, row b is ASAR data on regional (reg.) flight days only, and row c is ASAR data from farm-scale flight days.

Moreover, the results indicate a wet bias in the ASAR GM SSM relative to the field-collected data ($Bias_{\rm all} = 5.2\%$). Possible reasons for this could be residual moisture, porosity, and bulk density values used in the soil wetness to SM conversion or inaccuracies in the estimated dry and wet backscatter references. The SM range captured by the ASAR is relatively lower (on average $\sim$30%) than the *in situ* measurements (average SM dynamic $Range_{\rm field} = 0.31$ m^3/m^3 versus $Range_{\rm ASAR} = 0.21$ m^3/m^3).

The *in situ* SM data observed from the permanent SM stations were also used. To reduce possible georeferencing errors and the impact of the strong noise present in the ASAR images (ASAR GM mode showed a noise of $\sim$1.2 dB compared to $<$ 0.2 dB for the ASCAT data [26]), the ASAR GM SSM used for the comparisons was the average of a 2 $\times$ 2 window centered on the location of the station. Four out of the 18 permanent sites were not operational during the NAFE'05 campaign. In addition, SM data collected at K2 were very irregular for the month of November, resulting in only one day of coincident station–ASAR data collection. Therefore, K2 was excluded. Additionally, there were no data recorded at the time of the ASAR GM overpass at stations K4, M2, and M6; thus, the total number of working stations for the NAFE'05 period was further reduced to 11. The mean *in situ* SM values computed using station data collected within 2 h of the ASAR overpass time were used in the ASAR GM SSM–station SM analysis. Because of the close proximity, a daily average SM value for the S1–S7 stations was calculated and used in the analysis. Moreover, it should be noted that none of the stations were located in a forest area.

Fig. 2 (second row) shows spatial correlation between the station SM and ASAR GM SSM computed on per-pixel basis using all available coincident *in situ*–satellite observations within the PLMR regional flight box. While there was a good correlation with the station data at all station locations, $RMSE$ was better than 0.06 m^3/m^3 only at M3 and K3; no dependence on vegetation and topography was observed. A Pearson correlation coefficient of 0.75 indicated a good agreement between the two products (satellite and station SM) over the NAFE'05 domain (Fig. 2, plot 2a). Slightly higher correlation coefficients (Fig. 2, plots 2b and 2c) were computed for the two farm-scale sampling subareas ($Ra_1 = 0.76$ and $Ra_2 = 0.86$). Both subareas are similar in terms of vegetation (predominantly grasslands) and topography. The t-test was used to assess the difference in elevation and slope, indicating no significant difference between the two subunits at 95% confidence interval ($p > 0.05$).

The wet bias noticeable in the field–ASAR GM SSM comparison is also presented ($Bias_{\rm all} = 3.59\%$). The $RMSE$ was lower when using the station SM data (average $RMSE_{\rm station} = 0.085$ m^3/m^3) as compared to the field-measured SM data (average $RMSE_{\rm field} = 0.14$ m^3/m^3). This difference can be explained by the sampling frequency of the two data sets and the effect of the surface heterogeneity. Considering that SM is highly variable in space, a large number of observations are needed to achieve accurate average estimate within the satellite footprint. Over the NAFE'05 study domain (1600 km^2), stations are limited to (ideally) 18, and there is typically only one station present within a single ASAR GM pixel. Furthermore, at 1 km^2 (ASAR GM spatial resolution), having absolutely homogenous ground conditions is impossible. Thus, the stations do not actually provide an average estimate but a single SM measurement within the satellite footprint that is strongly controlled by the surface conditions present at the location of the station. Therefore, because of its higher sampling frequency, the field-collected data would more accurately capture the spatial variability within the satellite footprint, resulting into a more profound surface heterogeneity effect in the ASAR GM–field comparisons.

C. ASAR GM SSM–PLMR SM Comparisons

Spatial comparisons between ASAR GM SSM and PLMR-derived SM were carried out at several different scales. The results from these analyses are shown in Fig. 3. The scatter plots were built using all available observations acquired during the duration of the field campaign (see Table I). Two additional ASAR GM SSM–PLMR SM pairs were included: $ASAR_{\rm 19Nov} - PLMR_{\rm 18Nov}$ and $ASAR_{\rm 20Nov} - PLMR_{\rm 21Nov}$. The motivation for this choice of dates was due to the data availability.

The pixel-by-pixel comparison over the PLMR regional box at the original resolution of the two remote sensors (1-km resolution) was strongly affected by the high noise level of 1-km ASAR GM SSM product and resulted in $R = 0.39$ and

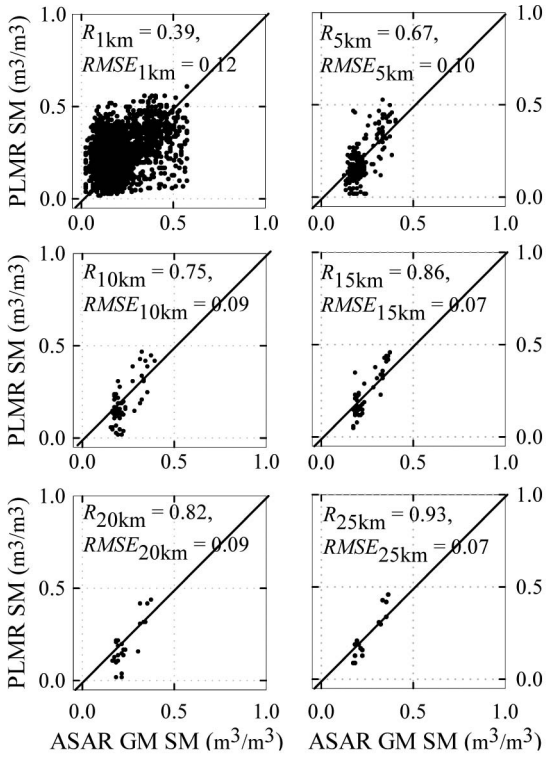

Note: n_{1km} = 2665, n_{5km} = 184, n_{10km} = 58, n_{15km} = 43, n_{20km} = 25, and n_{25km} = 15, where n is number of observations. All correlation values are significant at p = 0.01.

Fig. 3. PLMR versus ASAR GM SSM comparisons at several different scales: 1 (original pixel resolution), 5, 10, 15, 20, and 25 km. Pearson correlation coefficient (R) and root mean square error ($RMSE$) are given in the top portion of each scatter plot.

$RMSE = 0.12$ m^3/m^3. Decreasing the spatial resolution by aggregating the data resulted in R and $RMSE$ improvement, with the best R and $RMSE$ estimates achieved at 25 km [$R = 0.93$ and $RMSE = 0.07$ m^3/m^3 (Fig. 3)]. Although R increased significantly ($R = 0.67$) after aggregating the ASAR GM SSM up to 5 km, $RMSE$ remained close to the 1-km result. Despite the improved correlation coefficients at 10 and 15 km, the $RMSE$ remained high. If, however, the bias was removed [26], the error values improved, on average, by 10%, except at 1 km where the relative reduction in $RMSE$ was only 2.9%, and were as follows: 0.117 m^3/m^3 at 1 km, 0.088 m^3/m^3 at 5 km, 0.083 m^3/m^3 at 10 km, 0.069 m^3/m^3 at 15 km, 0.080 m^3/m^3 at 20 km, and 0.063 m^3/m^3 at 25 km. Even though the error values remained above the desired accuracy range, the results can be considered reasonable in terms of potential ASAR GM application for assimilation into hydrologic models, e.g., taking into account the high noise levels present in the 1-km data.

At finer spatial resolution, an important condition for good correlation is having a wide range of SM conditions (i.e., from very wet to very dry). This condition was not satisfied on an individual day. Moreover, the ASAR GM SSM range had a lower overall range compared to PLMR. Together, this resulted in poor daily correlations (Fig. 4). The mean here was thus computed as an average from the R values for each individual day. As can be seen, although the R_{mean} (black square in Fig. 4) indicates reasonable overall correlations between the

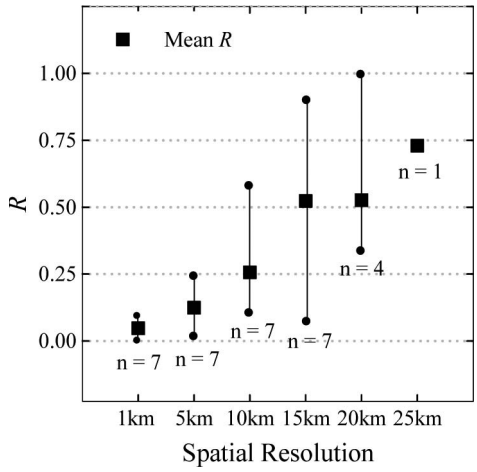

Fig. 4. Daily R-value variation with spatial resolution between ASAR GM SSM (m^3/m^3) and PLMR SM (m^3/m^3). Black solid squares show the average from paired days (n), whereas the upper and lower limits of the whiskers indicate, respectively, the minimum and maximum correlation coefficients at a particular spatial resolution.

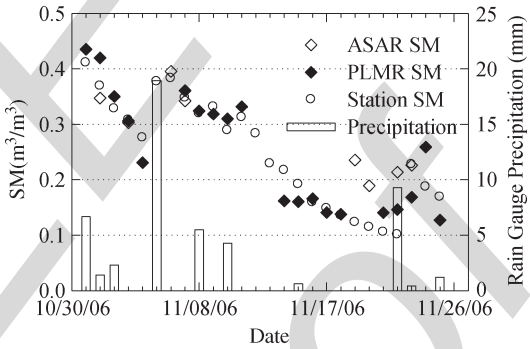

Fig. 5. (Solid diamonds) Mean daily ASAR GM, (white diamonds) PLMR, and (circles) station SM (m^3/m^3) products and (bars) rain gauge precipitation (mm) time series for the NAFE'05 duration. Each individual daily SM value was computed by spatially averaging all available observations within the aircraft flight box bounded by the white solid line in Fig. 1.

two sensors at coarser scale, there was a wide range of R variability on a daily basis, shown by the R_{min} and R_{max} (lower and upper limits of the whiskers in Fig. 4). One can notice consistent increase and slight drop at 20 km in the daily R_{mean} with a decrease in resolution which is similar to the results from the overall spatial analysis that were discussed in the previous paragraph (Fig. 3).

Wetting and drying trends are indicated by the response of both sensors (Fig. 5). The rapid increase in SM due to the October 31st and November 5th rainfall events followed by drying is in the same order of magnitude, showing a good agreement in the response of both systems. However, by the end of the observing period, the ASAR GM SSM exhibits a wet bias. The lack of ASAR data between November 8th and 18th does not allow interpretation of the ASAR GM SSM behavior under drying conditions and, thus, an examination of the wet bias dynamics. Taking into consideration the mean ASAR and PLMR SM ($PLMR_{\mathrm{NAFE05mean}} = 0.23$ m^3/m^3 and $ASAR_{\mathrm{NAFE05mean}} = 0.29$ m^3/m^3) values shown in Fig. 5, it can be assumed that the ASAR GM SSM values remain higher than the PLMR-derived SM values. The almost perfect agreement in the beginning of the time series (the wettest SM

TABLE II
DESCRIPTIVE STATISTICS AND TEMPORAL CORRELATION COEFFICIENTS FOR ASAR GM SSM AND PLMR SM PRODUCTS FOR THE DURATION OF THE NAFE'05 EXPERIMENT

Land Unit	Area (%)	# 1 km pixels	Descriptive Statistics: PLMR SM (m^3/m^3) avr.	PLMR SM st.dev	ASAR SM (m^3/m^3) avr.	ASAR SM st.dev	PLMR-SAR GM Temporal Correlation: # *days*	*R*	*RMSE* (m^3/m^3)
All	100	1801	0.25	0.07	0.28	0.09	5	0.989*	0.052
Grasslands	79.84	1438	0.25	0.06	0.28	0.09	5	0.996*	0.056
Croplands	1.44	26	0.34	0.06	0.28	0.08	5	0.676	0.134
Forestlands	18.71	337	0.17	0.03	0.27	0.09	5	0.775	0.142

Note: * Result is significant at p=0.01

conditions) and the large difference between ASAR and PLMR around November 18th and 19th suggest that the wet ASAR GM SSM bias is the strongest under dry ground conditions. This was further supported by the values computed using the limited number of available PLMR–ASAR GM coincident days, i.e., $Bias_{\mathrm{Nov1-7}} = 0.6\%$ versus $Bias_{\mathrm{Nov18-23}} = 8\%$ ($n = 4$ for both time periods, where n is the number of coincident days). However, we cannot generalize some of the conclusions due to the limited time duration examined here.

The ASAR and PLMR temporal correlation analysis is presented in Table II. Although the overall $RMSE$ here was low ($RMSE_{\mathrm{all}} = 0.052\ \mathrm{m}^3/\mathrm{m}^3$), when computed on a vegetation-type basis, the R and $RMSE$ values demonstrated some variability. Grasslands, which occupy ~80% of the domain, indicated a good temporal agreement with R of 0.996 and $RMSE$ of 0.056 $\mathrm{m}^3/\mathrm{m}^3$. Despite the reasonable R values for the croplands and forests, $RMSE$ values were on the order of 0.13–0.14 $\mathrm{m}^3/\mathrm{m}^3$, which may be due to the limited extent of these two cover classes and their homogeneity.

An example of spatial comparisons at 1, 5, and 10 km on a per-pixel basis between PLMR SM and ASAR GM SSM from November 7th and 6th (wet SM conditions following the rainfall event from November 5th) and November 20th and 21st (dry SM conditions associated with a ten-day dry-down period), respectively, is shown in Fig. 6. The PLMR SM map represents the area as being drier in the southern portion of the domain and wettest over the croplands. Due to the strong ASAR noise level at 1 km, that pattern cannot be seen as noticeably as on the PLMR image. Although there is a general resemblance between the two images, most of the ground patterns clearly visible in the PLMR-derived SM product are strongly masked by the noise present in the ASAR product. Several things need to be taken into account when interpreting these images: different time span between the rainfall event and the sensor dates (i.e., Nov. 5th—precipitation, Nov. 6th—ASAR GM, and Nov. 7th—PLMR). Additionally, ASAR GM and PLMR acquisitions were done at different times during the day (ASAR GM ~1000 P.M. versus PLMR ~1000 A.M). Furthermore, as already explained, both systems operate at different frequencies [shallower ASAR GM (C-band) sensing depth as compared to PLMR (L-band)]. Therefore, the more homogeneous wetting throughout the northern and the central portions of the domain observed in the ASAR GM SSM at 5 and 10 km was anticipated. Along with the previously listed factors, the poor resemblance over the southern one-third of the area, which is mainly occupied by forests, may be due to model parameterization inaccuracies (in both retrievals) for this

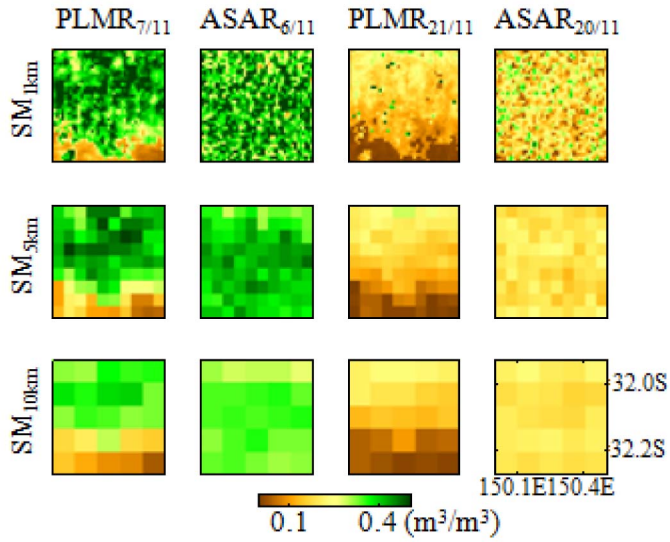

Fig. 6. Spatial comparisons between PLMR SM for November 7 and 21, 2005 and ASAR GM SSM for November 6 and 20, 2005 at 1-, 5-, and 10-km pixel resolutions.

particular vegetation class. The strong vegetation attenuation present under such conditions would deteriorate the SM signal and strongly increase the scattering in the case of ASAR. Furthermore, considering that, at the 1-km pixel, it is difficult to achieve uniform ground conditions, the measured signal would be additionally complicated by the existence of subpixel heterogeneity. The performed upscaling significantly reduced the noise present in the ASAR GM data, and a visible resemblance between both products emerged.

A common trend can be observed in Figs. 2, 3, and 5—ASAR GM lacks the dynamics captured in the other SM products described here. This is most noticeable in the ASAR GM–PLMR comparisons (Fig. 3), where the range is further reduced by the upscaling. At 1 km, the observed variability in the ASAR GM SSM data is caused by the high ASAR GM noise level, which, as discussed earlier, is the major source of error in the algorithm. The proposed spatial aggregation reduces the noise and thus improves the SM signal. The ASAR GM SSM range drops from 0.28 $\mathrm{m}^3/\mathrm{m}^3$ at 5 km to 0.20 $\mathrm{m}^3/\mathrm{m}^3$ at 15 km and remains constant onward, which leads to the suggestion that the proposed limits for spatial averaging to 3–10 km [26] may be higher. In addition, it appears that the satellite and the aircraft spatially compare better in the wet end than when drier, which is similar to the temporal trend in the series analysis shown in Fig. 5. Overall, the ASAR GM SSM demonstrates lower

sensitivity and, as pointed out earlier, exhibits a narrower SM range compared to the PLMR SM product. Uncertainties in the bulk density used for the relative-to-absolute SM conversion in the ASAR GM SSM case, along with inherited errors in the retrieval algorithms, can explain the large dynamic range difference between the ASAR GM and PLMR SM products (0.43 versus 0.22 m^3/m^3, where the values were computed as an average of the dynamic range at 5–25 km, excluding 1 km).

Finally, a significance test for R with $p = 0.01$ was performed in order to assess the statistical accuracy of the spatial (Figs. 2 and 3) and temporal (Table II) correlations achieved in this paper. All R values were found to be significant (except for the temporal coefficients computed over croplands and forestlands), which, in turn, confirms the previously discussed relationships and levels of agreement among the three SM products examined in this paper.

IV. Conclusion

The ASAR GM surface soil wetness product has been assessed for its sensitivity to SM using *in situ*observed (permanent stations and field-collected) and aircraft-derived SM over the NAFE'05 study area. The area is predominantly covered by grasslands and partly by forests and croplands. The ASAR GM SSM product was shown to capture the SM variability reasonably well when evaluated with the point measured *in situ* data obtained from the permanent SM stations in the domain ($R = 0.69$ and $RMSE = 0.099$ m^3/m^3). Comparisons with field-collected and PLMR-derived SM at 1-km SM showed similar correlation and root mean square error.

An important source of error in the ASAR GM SSM is the high noise level in the satellite system. Some of the noise effects and the additional impact of vegetation and topographic conditions were smoothed out by using a 2×2 window when extracting the ASAR GM SSM values corresponding to the station location. Several main conclusions can be noted.

1) Temporal analysis demonstrated good mean overall ASAR GM SSM sensitivity to SM at 1-km spatial scale and a wet bias compared to the *in situ* data for the duration and ground conditions of the NAFE'05 field campaign.
2) Comparisons with *in situ* SM data revealed high spatial agreement, which was not achieved when using the aircraft data set. Thus, it may be concluded that the spatial correlations were strongly dependent on the spatial scale at which the analysis was performed, and were largely controlled by the high ASAR GM noise levels.
3) Decrease in spatial resolution (increase in pixel size) resulted in the improvement in R and $RMSE$ shown to be the best at 25 km; however, $RMSE$ remained higher than desired for SM retrieval when using microwave techniques.
4) Temporal changes were adequately represented in both data sets showing wetting and drying patterns with an almost perfect agreement in the beginning of the campaign when the SM conditions were the wettest.

It should be noted that the results presented by Pathe *et al.* [26] are solely based on long-term temporal agreement. This analysis was focused primarily on evaluation of the ASAR GM SSM spatial accuracy at several different scales. Overall, this paper confirms the conclusion of Pathe *et al.* [26] that ASAR GM has potential for monitoring SM and verifies its ability to successfully depict change in moisture conditions. However, these results indicate that the proposed aggregation to a minimum of 3-km spatial resolution may be slightly underestimated. The presented results from the ASAR–PLMR comparisons at 1 km over the NAFE'05 ground conditions demonstrated that, despite the high spatial correlation coefficients and low $RMSE$ computed using point observed SM, detailed spatial pattern comparison was poor due to noise in the ASAR GM product. More research needs to be carried out in exploring techniques for reducing the noise, which may result in improved spatial pattern resemblance. This will further permit the use of the ASAR GM (or, in general, the use of any fine-resolution actively) derived product for disaggregation of coarse-resolution SM estimates through applying similar synergistic algorithms as the one proposed by [10]. Moreover, the upcoming SMAP mission is anticipated to provide radar data at 3-km ground spacing. However, the raw backscatter observations will be acquired at the same spatial resolution as ASAR GM, and as was demonstrated, at this resolution, there is a significant level of noise that will deteriorate the SM signal. Thus, the results of this paper support the SMAP-adopted approach for spatial averaging of the 1-km radar estimates to coarser aggregates.

Although the estimated error values were higher than the desired accuracy of 0.04 m^3/m^3, considering that several data assimilation techniques (i.e., Kalman filter/smoother and optimum interpolation) allow one to account for the observation and the model errors in the assimilation step suggests that ASAR GM has potential for data assimilation applications.

Acknowledgment

The authors would like to thank the European Space Agency (ESA) for kindly providing the ENVISAT ASAR GM data. The participation of I. Mladenova and V. Lakshmi in the National Airborne Field Experiment 2006 (NAFE'06) field campaign was made possible through funding by NASA NNX06AG85G (Program Manager Dr. J. Entin). The NAFE'05 was made possible through the Australian Research Council financial support by Grants DP0557543, LE0453434, and LE0560930. Initial setup and maintenance were funded by the Australian Research Council (DP0209724 and DP0556941) and NASA. The study of the ASAR GM SSM has been carried out within the framework of the SHARE project funded by the ESA.

References

[1] Y. Oh, K. Sarabandi, and F. T. Ulaby, "An empirical model and an inversion technique for radar scattering from bare soil surfaces," *IEEE Trans. Geosci. Remote Sens.*, vol. 30, no. 2, pp. 370–381, Mar. 1992.

[2] A. K. Fung, Z. Li, and K. S. Chen, "Backscatter from a randomly rough dielectric surface," *IEEE Trans. Geosci. Remote Sens.*, vol. 30, no. 2, pp. 356–369, Mar. 1992.

[3] F. T. Ulaby, K. Sarabandi, K. McDonald, M. Whitt, and M. C. Dobson, "Michigan microwave canopy scattering model," *Int. J. Remote Sens.*, vol. 11, no. 7, pp. 1223–1253, Jul. 1990.

[4] M. S. Moran, S. McElroy, J. M. Watts, and L. C. D. Peters, "Radar remote sensing for estimation of surface soil moisture at the watershed scale," in *Modeling and Remote Sensing Applied in Agriculture (US and Mexico)*, C. W. Richardson, A. S. Baez-Gonzalez, and M. Tiscareno, Eds. Aguascalientes, Mexico: INIFAP Publ., Oct. 2006, ch. 7, pp. 91–106.

[5] W. Wagner and K. Scipal, "Large-scale soil moisture mapping in Western Africa using ERS scatterometer," *IEEE Trans. Geosci. Remote Sens.*, vol. 38, no. 4, pp. 1777–1782, Jul. 2000.
[6] W. Wagner, J. Noll, M. Borgeaud, and H. Rot, "Monitoring soil moisture over the Canadian Prairies with the ERS scatterometer," *IEEE Trans. Geosci. Remote Sens.*, vol. 37, no. 1, pp. 206–216, Jul. 1999a.
[7] W. Wagner, G. Lemoine, M. Borgeaud, and H. Rott, "A study of vegetation cover effects on ERS scatterometer data," *IEEE Trans. Geosci. Remote Sens.*, vol. 37, no. 2, pp. 938–948, Mar. 1999b.
[8] W. Wagner, G. Lemoine, and H. Rott, "A method for estimating soil moisture from ERS scatterometer and soil data," *Remote Sens. Environ.*, vol. 70, no. 2, pp. 191–207, Nov. 1999c.
[9] Z. Bartalis, W. Wagner, V. Naeimi, S. Hasenauer, K. Scipal, H. Bonekamp, J. Figa, and C. Anderson, "Initial soil moisture retrievals form the METOP-A Advanced Scatterometer (ASCAT)," *Geophys. Res. Lett.*, vol. 34, no. 20, p. L20 401, Oct. 2007, DOI:10.1029/2007GL031088.
[10] U. Narayan, V. Lakshmi, and T. Jackson, "High-resolution change estimation of soil moisture using L-band radiometer and radar observations made during the SMEX04 experiment," *IEEE Trans. Geosci. Remote Sens.*, vol. 40, no. 6, pp. 1545–1554, Jun. 2006.
[11] J. P. Walker and P. R. Houser, "A methodology for initializing soil moisture in a global climate model: Assimilation of near-surface soil moisture observations," *J. Geophys. Res.*, vol. 106, no. D11, pp. 11 761–11 774, Jun. 2001.
[12] A. A. Berg, J. S. Famiglietti, J. P. Walker, and P. R. Houser, "Impact of bias correction to reanalysis products on simulation of North American soil moisture and hydrological fluxes," *J. Geophys. Res.*, vol. 108, no. D16, p. 4490, 2003.
[13] R. H. Reichle, R. D. Koster, J. Dong, and A. A. Berg, "Global soil moisture from satellite observations, land surface models, and ground data: Implications for data assimilation," *J. Hydrometeorol.*, vol. 5, no. 3, pp. 430–442, Jun. 2004.
[14] W. Ni-Meister, P. R. Houser, and J. P. Walker, "Soil moisture initialization for climate prediction: Assimilation of scanning multifrequency microwave radiometer soil moisture data into a land surface model," *J. Geophys. Res.*, vol. 111, no. D20, p. D20 102, Oct. 2006, DOI:10.1029/2006JD007190.
[15] R. H. Reichle, R. D. Koster, P. Liu, S. P. P. Mahanama, E. G. Njoku, and M. Owe, "Comparison and assimilation of global soil moisture retrievals from the Advanced Microwave Scanning Radiometer for the Earth Observing System (AMSR-E) and the Scanning Multichannel Microwave Radiometer (SMMR)," *J. Geophys. Res.*, vol. 112, no. D9, p. D09 108, May 2007, DOI:10.1029/2006JD008033.
[16] R. C. Pipunic, J. P. Walker, and A. Western, "Assimilation of remotely sensed data for improved latent and sensible heat flux prediction: A comparative synthetic study," *Remote Sens. Environ.*, vol. 112, no. 4, pp. 1295–1305, Apr. 2008.
[17] R. Panciera, J. P. Walker, J. D. Kalma, E. J. Kim, J. M. Hacker, O. Merlin, M. Berger, and N. Skou, "The NAFE'05/CoSMOS data set: Toward SMOS soil moisture retrieval, downscaling, and assimilation," *IEEE Trans. Geosci. Remote Sens.*, vol. 46, no. 3, pp. 736–745, Mar. 2008.
[18] R. Panciera, J. P. Walker, J. D. Kalma, E. J. Kim, K. Saleh, and J.-P. Wigneron, "Evaluation of the SMOS L-MEB passive microwave soil moisture retrieval algorithm," *Remote Sens. Environ.*, vol. 113, no. 2, pp. 435–444, Feb. 2009.
[19] C. Rüdiger, G. Hancock, H. M. Hemakumara, B. Jacobs, J. D. Kalma, C. Martinez, M. Thyer, J. P. Walker, T. Wells, and G. R. Willgoose, "Goulburn river experimental catchment data set," *Water Resour. Res.*, vol. 43, no. 10, p. W10 403, 2007.
[20] R. Panciera, O. Merlin, R. Young, and J. P. Walker, *The Hydroprobe Data Acquisition System (HDAS): User Manual*. Melbourne, Australia: Univ. Melbourne, Oct. 2006.
[21] R. Panciera, J. P. Walker, O. Merlin, J. D. Kalma, and E. J. Kim, "Scaling properties of L-band passive microwave soil moisture: From SMOS to paddock scale," in *Proc. 30th Hydrol. Water Resour. Symp.*, Launceston, Australia, Dec. 4–7, 2006.
[22] J.-P. Wigneron, Y. Kerr, P. Waldteufel, K. Saleh, M.-J. Escorihuela, P. Richaume, P. Ferrazzoli, P. de Rosnay, R. Gurney, J.-C. Calvet, J. P. Grant, M. Guglielmetti, B. Hornbuckle, C. Mätzler, T. Pellarin, and M. Schwank, "L-band Microwave Emission of the Biosphere (L-MEB) model: Description and calibration against experimental data sets over crop fields," *Remote Sens. Environ.*, vol. 107, no. 4, pp. 639–655, Apr. 2007.
[23] T. Mo, B. J. Choudhury, T. J. Schmugge, and T. J. Jackson, "A model from the microwave emission of vegetation-covered fields," *J. Geophys. Res.*, vol. 87, no. 11, pp. 229–237, 1982.
[24] M. C. Dobson, F. T. Ulaby, M. T. Hallikainen, and M. A. El-Rayes, "Microwave dielectric behavior of wet soil—Part II: Dielectric mixing models," *IEEE Trans. Geosci. Remote Sens.*, vol. GRS-23, no. 1, pp. 35–36, Jan. 1985.
[25] C. Mätzler, "Microwave permittivity of dry sand," *IEEE Trans. Geosci. Remote Sens.*, vol. 36, no. 1, pp. 317–319, Jan. 1998.
[26] C. Pathe, W. Wagner, D. Sabel, M. Doubkova, and J. Basara, "Using ENVISAT ASAR global mode data for surface soil moisture retrieval over Oklahoma, USA," *IEEE Trans. Geosci. Remote Sens.*, vol. 47, no. 2, pp. 468–480, Feb. 2009.
[27] W. Wagner, C. Pathe, M. Doubkova, D. Sabel1, A. Bartsch, S. Hasenauer, G. Blöschl, K. Scipal, J. Martínez-Fernández, and A. Löw, "Temporal stability of soil moisture and radar backscatter observed by the Advanced Synthetic Aperture Radar (ASAR)," *Sensors*, vol. 8, pp. 1174–1197, 2008.
[28] C. Albergel, C. Rüdiger, D. Carrer, J.-C. Calvet, N. Fritz, V. Naeimi, Z. Bartalis, and S. Hasenauer, "An evaluation of ASCAT surface soil moisture products with *in situ* observations in Southwestern France," *Hydrol. Earth Syst. Sci.*, vol. 13, no. 2, pp. 115–124, 2009.
[29] M. T. van Genuchten, "A closed-form equation for predicting the hydraulic conductivity of unsaturated soils," *Soil Sci. Soc. Amer. J.*, vol. 44, no. 5, pp. 892–898, Sep. 1980.
[30] D. Hillel, *Environmental Soil Physics, Fundamentals, Applications, and Environmental Considerations*. New York: Academic, 1998.
[31] R. Hoeben, P. A. Troch, Z. Su, M. Mancini, and K.-S. Chen, "Sensitivity of radar backscattering to soil surface parameters: A comparison between theoretical analysis and experimental evidence," in *Proc. IGARSS*, Aug. 3–8, 1997, vol. 3, pp. 1368–1370.

Iliana Mladenova received the M.S. degree in hydrology and ecohydrology, with an emphasis in remote sensing, from the Vrije Universiteit, Amsterdam, The Netherlands, in 2006 and the Ph.D. degree in the same area from the University of South Carolina, Columbia, in 2009.

Between fall 2004 and spring 2006, she was with the Hydrology and Remote Sensing Laboratory, United States Department of Agriculture, Beltsville, MD, and in 2008, she spent three months with the Department of Civil and Environmental Engineering, Melbourne, Australia, focusing on studies in support of soil moisture algorithm development and validation, and downscaling issues. She is currently a Physical Research Scientist with the Hydrology and Remote Sensing Laboratory. She has an extensive experience in large-scale satellite and aircraft remote sensing validation experiments in support of NASA's AMSR-E and ESA's SMOS missions. Her research interests include microwave remote sensing of soil moisture, data assimilation, and remote sensing application in hydrology and agriculture.

Dr. Mladenova is a member of the IEEE Geoscience and Remote Sensing Society and the American Geophysical Union.

Venkat Lakshmi (S'94–M'99–SM'02) received the B.S. degree in civil engineering from the University of Roorkee, Roorkee, India, in 1987, the M.S. degree in civil and environmental engineering from the University of Iowa, Iowa City, in 1989, and the M.A. degree in civil engineering and the Ph.D. degree in operations research from Princeton University, Princeton, NJ, in 1995.

He has been working in remote sensing and modeling of the land surface hydrological cycle for the past 20 years on various aspects. These range from catchment hydrology to continental-scale hydrology and climate using data from aircraft sensors as well as satellites. He is currently a Professor with and the Chairman of the Department of Earth and Ocean Sciences, University of South Carolina, Columbia. He has served as an Associate Editor for the *Journal of Geophysical Research* and the *Journal of Water Resources Research* and was an Editor for hydrology for the American Geophysical Union (AGU) publication EOS. He is currently an Associate Editor for the *Journal of Hydrology*.

Dr. Lakshmi has served as the Chairman of the AGU Remote Sensing Committee for the Hydrology Section. He was one of the Founding Chairs of the IEEE GRSS User Applications Committee and has served on the Technical Paper Committee and chaired sessions at the IEEE International Geoscience and Remote Sensing Symposium.

Jeffrey P. Walker received the B.Surv. and B.E. (Civil) degrees from the University of Newcastle, Newcastle, Australia, in 1995, and the Ph.D. degree in environmental engineering from the same university in 1999.

He then joined the Hydrological Sciences Branch, NASA Goddard Space Flight Center, as a Visiting Scientist for two years, before joining the Department of Civil and Environmental Engineering, University of Melbourne, Melbourne, Australia. He is internationally recognized as a Leader in the fields of soil moisture remote sensing and data assimilation, using state-of-the-art models, airborne remote sensing infrastructure, and data assimilation techniques.

Rocco Panciera was born in Trento, Italy, in 1975. He received the M.S. degree in environmental engineering from the University of Trento, Trento, in 2003 and the Ph.D. degree in environmental engineering from the University of Melbourne, Melbourne, Australia, in 2009.

He is currently a Research Fellow with the Department of Civil and Environmental Engineering, University of Melbourne. His research is focused on remote sensing of soil moisture for environmental modeling from the future generation of passive microwave remote sensing platforms, such as SMOS and SMAP. Between 2005 and 2006, he led the series of extensive field campaigns conducted in southeastern Australia within the National Airborne Field Experiment.

Wolfgang Wagner (M'98–SM'07) was born in Wels, Austria, in 1969. He received the Dipl.-Ing. (M.Sc.) degree in physics and the Dr.techn. (Ph.D.) degree in remote sensing, both with excellence, from the Vienna University of Technology (TU Wien), Vienna, Austria, in 1995 and 1999, respectively. In support of his M.Sc. and Ph.D. studies, he received fellowships to carry out research at the University of Bern, Berne, Switzerland; Atmospheric Environment Service Canada; NASA Goddard Space Flight Centre; European Space Agency; and the Joint Research Centre of the European Commission.

From 1999 to 2001, he was with the German Aerospace Agency (DLR), where he was first a Project Assistant with the Institute of High Frequency Technology and later the Head of the SAR Applications team at the German Remote Sensing Data Centre. In 2001, he was appointed Professor for remote sensing with the Institute of Photogrammetry and Remote Sensing, TU Wien, where he has been the Head of the institute since 2006. His main research interests lie in geophysical parameter retrieval techniques from remote sensing data and application development. He focuses on active remote sensing techniques, in particular scatterometry, SAR, and airborne laser scanning.

Dr. Wagner is a member of the Science Advisory Groups for SMOS (ESA) and METOP ASCAT (EUMETSAT and ESA) and serves as ISPRS Commission VII President (2008–2012).

Marcela Doubkova was born in the Czech Republic in 1980. She studied geography at the Charles University, Prague, Czech Republic, in 2000–2003 and at the University of Nebraska, Lincoln, in 2003–2006. She received the M.S. degree in geography from the University of Nebraska, in 2006. In her M.S. thesis, she investigated the vegetation and soil water interactions with the use of microwave and optical data.

Since April 2007, she has been a Radar and Geographic Information System Analyst with the Institute of Photogrammetry and Remote Sensing, Vienna University of Technology, Vienna, Austria. Since June 2009, she has been one of the University Assistants of the institute. Her main research interest encompasses the study of vegetation biomass and water in soil and vegetation by use of microwave remote sensing.